Journal of Alloys and Compounds 509 (2011) 4132–4137

Contents lists available at ScienceDirect

Journal of Alloys and Compounds

journal homepage: www.elsevier.com/locate/jallcom

Formation of CuO nanorods and their bundles by an electrochemical dissolution and deposition process

Buppachat Toboonsung[a], Pisith Singjai[a,b,*]

[a] Department of Physics and Materials Science, Faculty of Science, Chiang Mai University, Chiang Mai 50200, Thailand
[b] Materials Science Research Center, Faculty of Science, Chiang Mai University, Chiang Mai 50200, Thailand

ARTICLE INFO

Article history:
Received 9 October 2010
Received in revised form
23 December 2010
Accepted 24 December 2010
Available online 31 December 2010

Keywords:
Electrochemical dissolution and deposition
Heat treatment
Copper oxide
Nanorods
Photoluminescence

ABSTRACT

Copper oxide nanorods (NRs) and their bundles were deposited on glass substrates by an electrochemical dissolution and deposition process. Changes in the electrode separation, the deposition time and the voltage could be used to control the morphologies, the thickness and the ratio of bundles/NRs. The formation of the NRs and their bundles was explained by an aggregation mechanism. A transformation of the Cu phase in the as-deposited sample to a single CuO phase was effected by an annealing treatment at 500 °C. The increasing photoluminescence (PL) intensity of the annealed sample resulted from a grain size growth and an improvement in the crystallinity.

1. Introduction

Cupric oxide (CuO) nanostructures (NSs) have received much attention because of their p-type semiconductor with energy gap of 1.2 eV [1]. CuO NSs are regarded as promising materials for many potential applications such as electrodes in dye-sensitized solar cells [2,3], capacitors [4], gas sensors, field effect transistors [5], anode materials for lithium-ion batteries [6], antimicrobials [7], humidity sensors [8] and diodes [9]. A number of synthesis methods for CuO NSs have been detailed in the literature, for example thermal plasma [6], hydrothermal [10], sparking [11,12], electroplating of copper (Cu) thin films with thermal annealing [13], electrochemical [14], sol–gel [15], thermal evaporation [16] and pulsed laser deposition [17]. Electrochemical methods for the formation of CuO NSs are of particular interest due to the many advantages over other methods including its low cost, ease of process and the various available types of electrolyte [18]. Furthermore, the electrochemical method allows the formation of diverse forms of CuO NSs, including cauliflower-shaped [4], honeycomb-shaped [8], nanorods (NRs) and nanospindles [18].

In this work, a method for the formation of CuO NSs was reported. The experiments were carried out by electrochemical dissolution, deposition and thermal annealing. The as-deposited and annealed CuO NRs were characterized using scanning electron microscopy (SEM), transmission electron microscopy (TEM), Raman spectroscopy, X-ray diffraction (XRD) and photoluminescence (PL).

2. Experimental details

Copper and stainless steel plates with sizes of $1.5 \times 5.0 \times 0.04\,cm^3$ were used as an anode and a cathode, respectively [18]. A glass substrate with a size of $0.5 \times 2.2 \times 0.016\,cm^3$ was attached on the cathode for deposition of the NSs, as shown in Fig. 1. The two electrodes were immersed in 100 ml of deionized water and a voltage of 10–30 V DC was applied [19,20]. The electrochemical dissolution and deposition were performed by varying the electrode separations from 2 to 10 mm and the deposition time from 1 to 8 h. The as-deposited samples were dried for 1 h and annealed at 300–500 °C for 30 min in an atmosphere of air [14]. Morphology of the films was characterized by scanning electron microscopy (SEM, JEOL JSM-6335F). Crystal structures were analyzed by transmission electron microscopy (TEM, JEOL JEM-2010), operated at 200 kV, Raman spectroscopy (Ar ion laser excitation 514.5 nm, power laser 0.5 mW, HORIBA JOBIN YVON T64000) and X-ray diffraction (XRD, Bruker D8 Advance). Optical properties were measured using a photoluminescence (PL) spectrometer (Perkin-Elmer LS50B) with a 290 nm excitation wavelength at room temperature.

3. Results and discussion

Fig. 2 shows the relationship between the current and the deposition time for samples prepared with a voltage of 10 V at various

* Corresponding author at: Department of Physics and Materials Science, Faculty of Science, Chiang Mai University, Chiang Mai 50200, Thailand.
Tel.: +66 53 941922x610; fax: +66 53 892271.
E-mail address: singjai@chiangmai.ac.th (P. Singjai).

0925-8388/$ – see front matter © 2011 Elsevier B.V. All rights reserved.
doi:10.1016/j.jallcom.2010.12.180

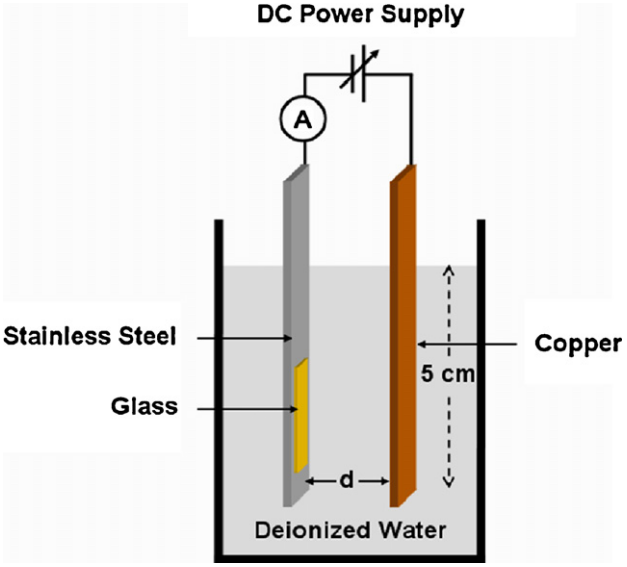

Fig. 1. Schematic diagram of the electrochemical dissolution and deposition processes.

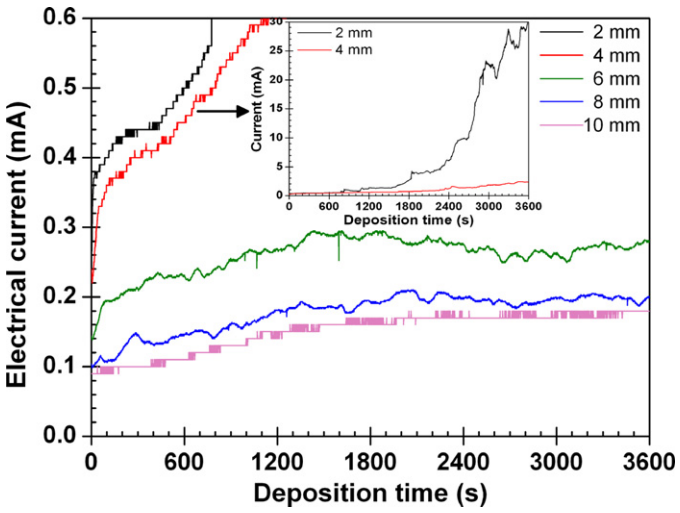

Fig. 2. The relationship between current and deposition time for various electrode separations. All measurements were taken with an applied voltage of 10 V.

electrode separations. It was revealed that the current increased with decreasing electrode separation. Furthermore, a rapid increase in current with time was observed at electrode separations of 2 and 4 mm (inset), whereas the current increased more slowly with time at electrode separations of 6–10 mm. It is noted that a steady

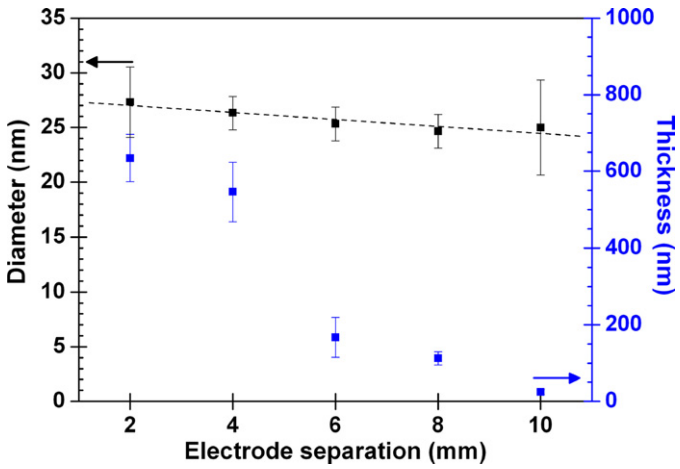

Fig. 4. Diameter of NRs and thickness of the as-deposited samples as function of the electrode separation from 2 to 10 mm with voltage of 10 V and deposition time of 1 h.

current was observed at the electrode separation of 8 mm. The morphologies of samples were characterized by cross-sectional SEM images, as shown in Fig. 3. It was revealed that the thickness decreased with increasing electrode separation, corresponding to a measured reduction in current with increasing electrode separation. Consequently, a maximum thickness of approximately 635 nm was observed at the higher current and a minimum thickness of approximately 25 nm was found at the lower current. Nevertheless, when current increased rapidly made non-uniformly film, uniform film with steady current at the electrode separation of 8 mm. The diameter of the as-deposited samples decreased linearly with increasing electrode separation whereas the thickness decreased exponentially, as shown in Fig. 4. It is noted that the uniformity of the thickness and the homogeneity of the NRs were affected by the stability of the current during the process [21]. However, the reproducibility of this result was confirmed by several repeated experiments.

Fig. 5a and b shows SEM images of the as-deposited films (fixed at an electrode separation of 8 mm and voltage of 10 V) for deposition times of 1 and 8 h, respectively. After a deposition time of 1 h only NRs are observed, while after 8 h NRs and bundles are present. The diameter of NSs (NRs and bundle NRs) as a function of the deposition time is shown in Fig. 6a. Interestingly, only rod-like shapes (defined as having a mean diameter in the range 25–40 nm) were found for the deposition times of 1 and 2 h, whereas a mixture of NRs and their bundles (defined as having a mean diameter in the range 40–110 nm) were observed for the deposition times of 3–8 h. It is also noted that the diameters of both forms and the ratio of bundle/NRs increased linearly with increasing deposition time, as shown in Fig. 6a and b. It was found that the ratio increased

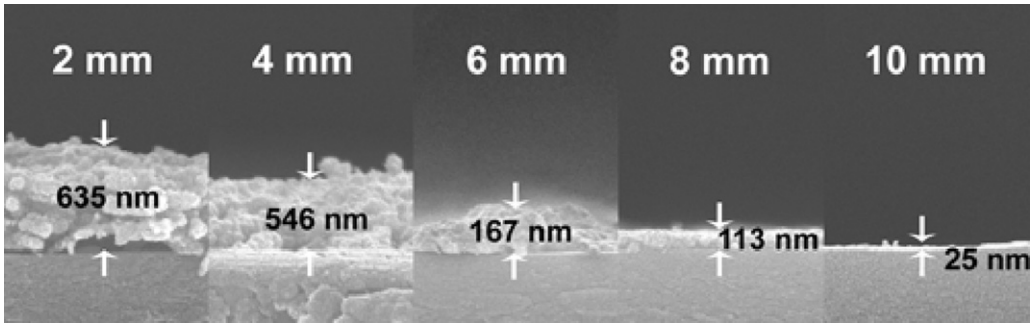

Fig. 3. Cross-sectional SEM images of the as-deposited samples prepared with a voltage of 10 V and at various electrode separations.

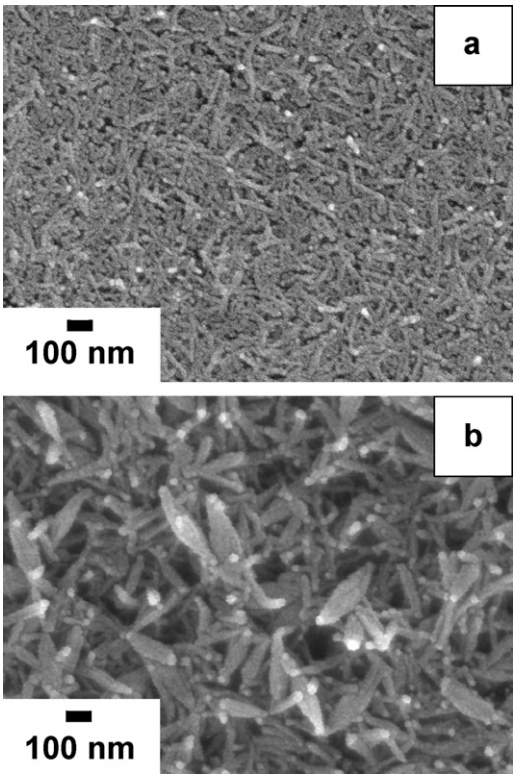

Fig. 5. SEM images of the as-deposited samples prepared with an electrode separation of 8 mm, applied voltage of 10 V and deposition time of (a) 1 h and (b) 8 h.

with decreasing electrode separation and the maximum ratio was obtained at an electrode separation of 2 mm and a voltage of 20 V, as shown in Fig. 6c. In other words, the ratio could be controlled by choosing the deposition time, the electrode separation and the applied voltage.

Fig. 7a shows a low magnification TEM image of the as-deposited NRs, while the inset shows a high magnification TEM image of the same sample. It is observed that an individual NR consists of randomly aggregated NPs whereas a bundle consists of NRs, as shown in Fig. 7b. The selected area electron diffraction (SAED) pattern of the as-deposited bundle indicates that the films exhibit (1 1 1), (2 2 0) and (3 1 1) planes of Cu and $(\bar{1}\,1\,1)$, (0 2 0), (0 2 1), (2 2 1), $(\bar{2}\,2\,1)$ and $(\bar{1}\,1\,3)$ planes of CuO, as shown inset in Fig. 7b. TEM images with a corresponding SAED pattern (inset) of the sample annealed at 300 °C and 500 °C for 0.5 h are shown in Fig. 7c and d, respectively. It is evident that the NRs aggregated into a bundle from which a spindle was formed [18,19]. The SAED pattern shows that the annealed copper oxide NRs at 300 °C consist of Cu_2O and CuO, whereas the annealed sample at 500 °C consists only of the CuO phase with a monoclinic structure, as identified by: $(\bar{1}\,1\,1)$, (1 1 1), (1 1 2) and (2 0 2) planes.

The morphology of CuO NSs synthesized by electrochemical methods usually depends on the oxidation rate and the solution used in the process. Generally, aggregation of CuO NPs is explained by a growth of CuO NRs by an oriented aggregation mechanism [18,19,22]. This aggregation mechanism occurs when removed and/or adsorbed molecules of a solvent connect through chemical bonding and reduce the interfacial energy between primary particles. The secondary particles produced from the attachment and oriented aggregation of the primary particles then form as new single crystals or artificial crystals [22,23]. However, we explain the formation of the single NRs into bundles described here by a different mechanism, which is as follows: Firstly, Cu plate was dissolved to Cu^{2+}, and this combined with hydroxyl groups from deionized water to form $Cu(OH)_2$ NRs, which were confirmed in the inset TEM image in Fig. 7a. Next, the tiny NPs aggregated randomly around a single NR in solution due to reduced surface energy, and the deposi-

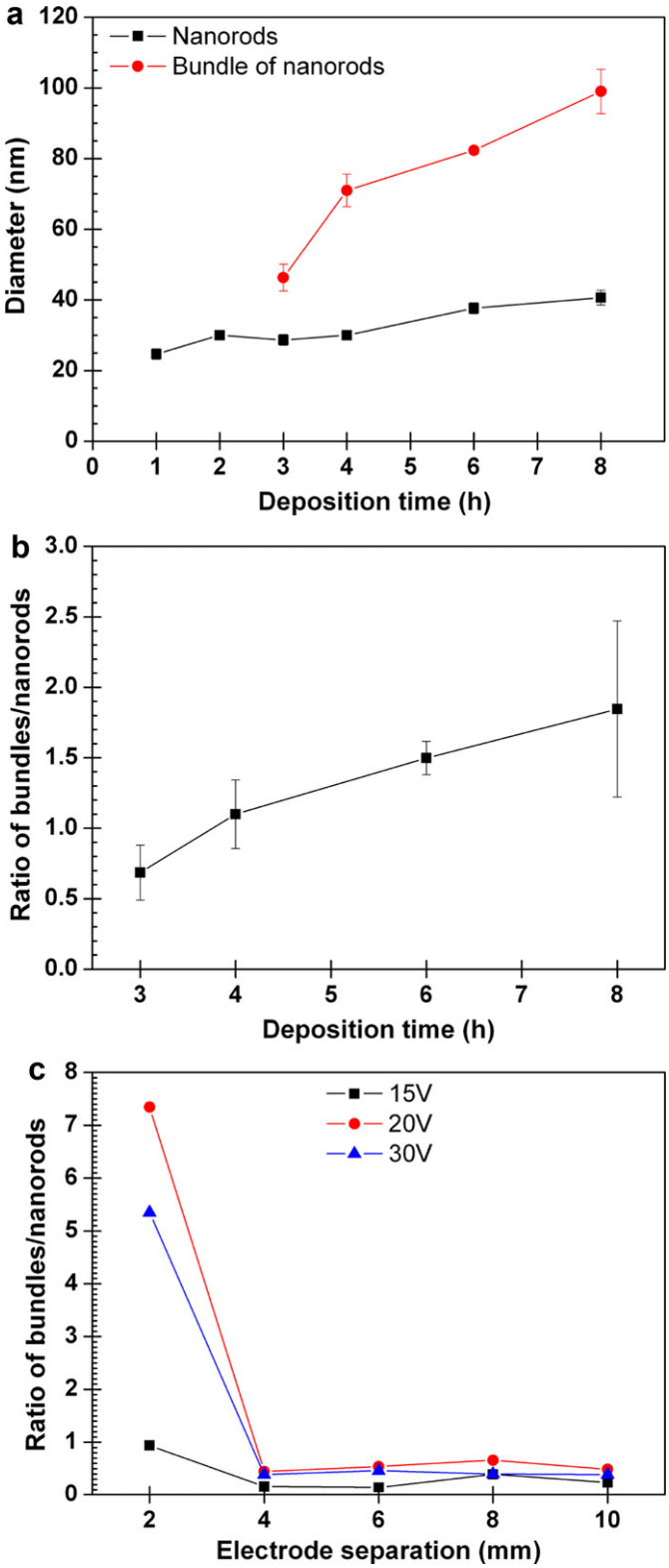

Fig. 6. (a) Diameter of CuO NSs, (b) the ratio of bundles/NRs as function of the deposition time, prepared at an electrode separation of 8 mm, a voltage of 10 V and (c) the ratio of bundles/NRs as function of the electrode separation, with an applied voltage of 15–30 V and a deposition time of 1 h.

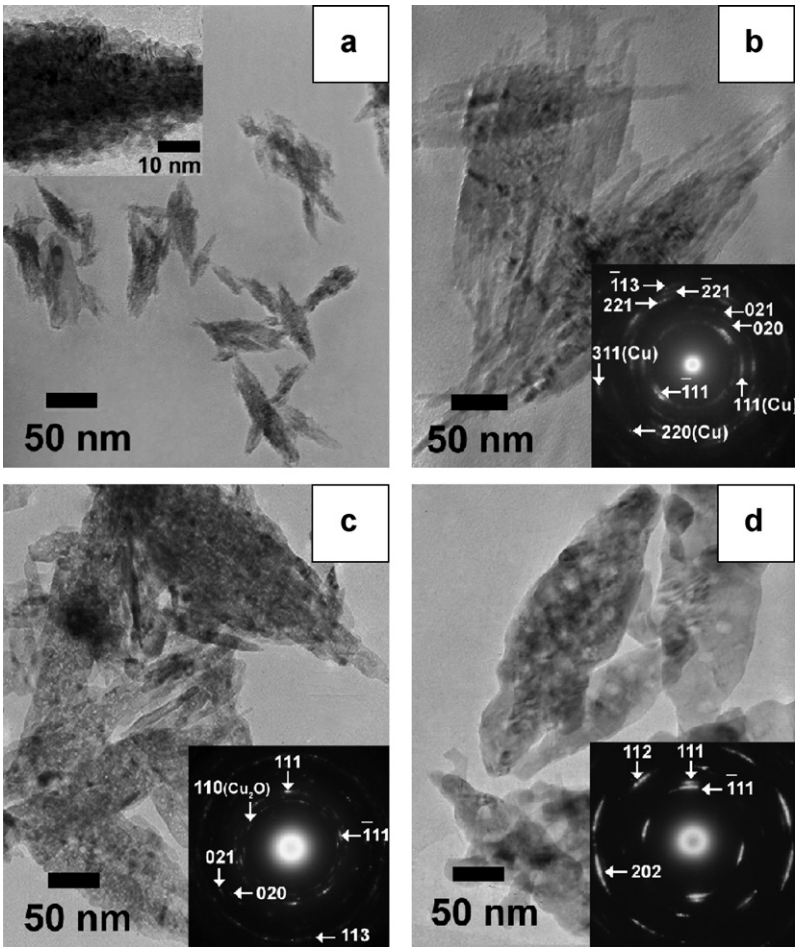

Fig. 7. TEM images of the as-deposited copper oxide NSs illustrated in Fig. 5: (a) NRs (inset TEM image high magnification of NRs) with (b) bundle NRs (inset associated SAED pattern) and annealed bundle NRs (inset associated SAED pattern) at temperatures of (c) 300 °C with (d) 500 °C.

tion of nanorods on the cathode surface began between deposition times of 0 and 2 h, which is confirmed by the TEM image in Fig. 7a [22]. Finally, at deposition times over 2 h, aggregations of many NR formed into bundles, as confirmed by the TEM image shown in Fig. 7b. [18,19]. The mechanism that results in the transformation in shape from NPs to bundles of NRs is summarized in Fig. 8.

Fig. 9 shows XRD spectra for the as-deposited bundled NRs for 8 h and the annealed bundled NRs (with the annealing carried out at a temperature of 300–500 °C for 0.5 h) prepared at an electrode separation of 8 mm with a deposition time of 8 h. It is known that the heat treatment process introduces oxygen into the films [24]. The XRD spectrum consisted of a strong phase of Cu and weak phase of CuO for the as-deposited sample. During the annealing of the sample at a temperature of 300 °C, the Cu phase received oxygen and transformed to the Cu_2O phase. It is noted that the XRD intensity of the Cu_2O phase decreased with increasing in the annealing tem-

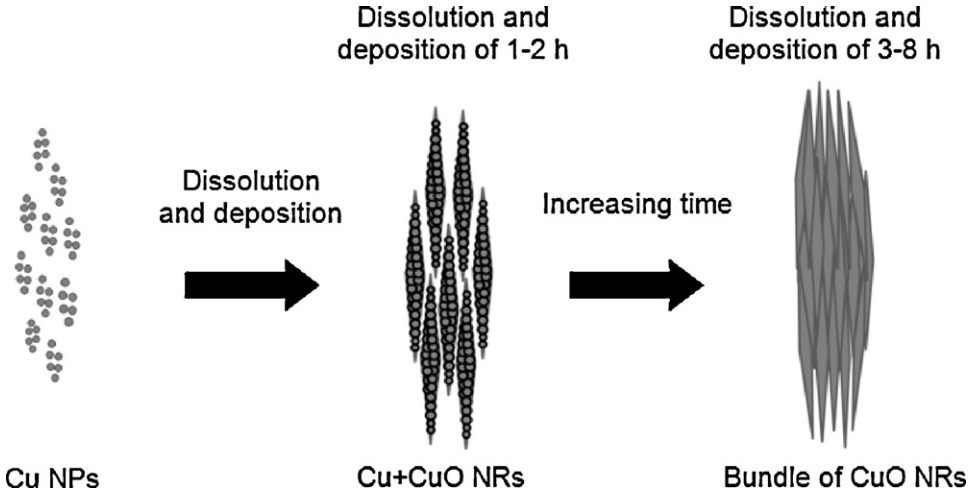

Fig. 8. Schematic diagrams of the growth mechanism of NRs into their bundles.

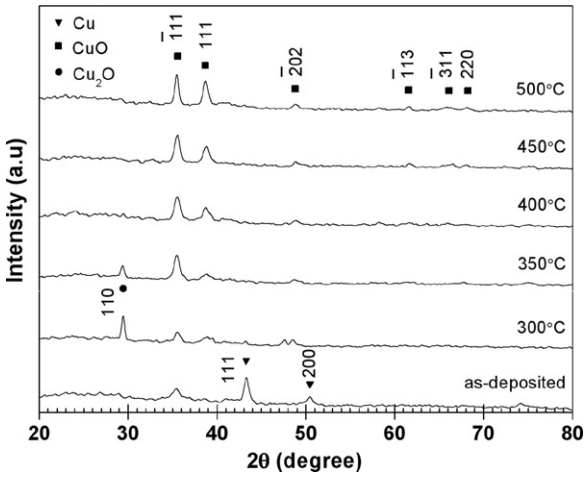

Fig. 9. XRD spectra of the as-deposited sample and the annealed CuO NSs with annealing temperatures from 300 to 500 °C and 0.5 h annealing time.

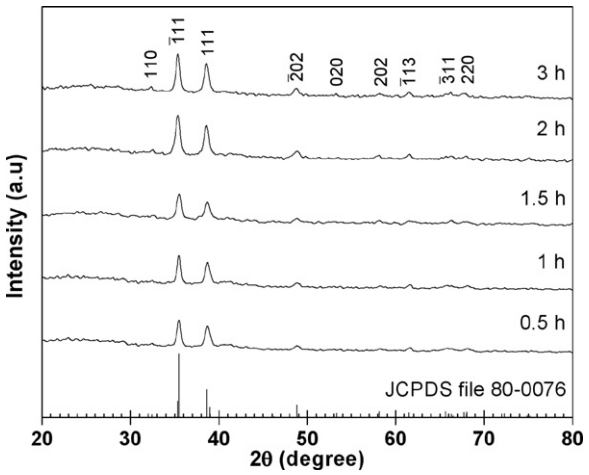

Fig. 11. XRD spectra for the annealed CuO NSs, annealed at 500 °C for 0.5–3 h.

perature from 350 °C to 400 °C. The Cu_2O phase was transformed completely at 500 °C, resulting in a single CuO phase.

Fig. 10 shows Raman spectra for the as-deposited sample for 8 h and the annealed samples (annealed at 400–500 °C for 0.5 h). Three Raman active modes ($A_g + B_g^1 + B_g^2$) of the as-deposited sample were observed through three Lorentzian peak fits which showed peak centers at approximately 303, 353 and 629 cm^{-1}, respectively. Three Lorentzian peak fits of the annealed CuO NSs (annealed at 500 °C) showed peak centers at approximately 298, 348 and 633 cm^{-1}, corresponding to a CuO phase [25]. Two Raman peak centers for A_g and B_g^1 modes of the as-deposited samples were observed to be blue-shifted while the peak center of the B_g^2 mode was observed to be red-shifted when compared with the annealed CuO NSs [26,27]. The blue-shift of the peaks occurred as a result the longitudinal size and high aspect ratio of the NRs from as-deposited samples whereas the red-shift of Raman peak was explained by the phonon confinement effect [26,27].

Fig. 11 shows XRD spectra for the CuO NSs single phase for annealing times from 0.5 to 3 h at 500 °C. It is noted that the XRD intensity of the CuO phase increased with increasing annealing time. The peaks of CuO phase: $(\bar{1}\,1\,1)$, $(1\,1\,1)$, $(\bar{2}\,1\,1)$, $(\bar{1}\,1\,3)$, $(\bar{3}\,1\,1)$ and $(2\,2\,0)$ planes indicated a monoclinic structure with lattice constants $a = 4.6797$ Å, $b = 3.4314$ Å and $c = 5.1362$ Å (JCPDS file number 80-0076). These XRD data are in good agreement with the SAED pattern results.

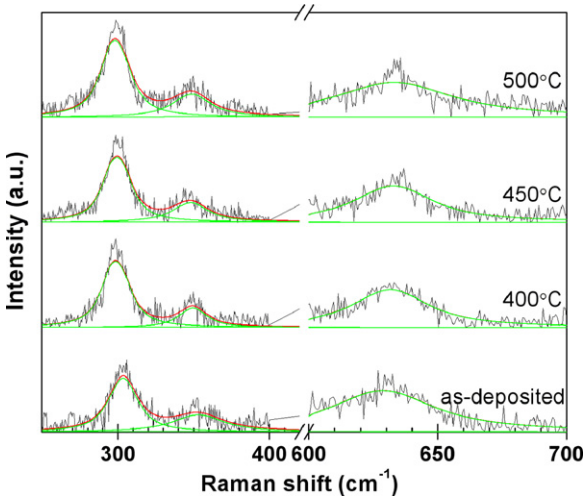

Fig. 10. Raman spectra for the as-deposited sample and the annealed CuO NSs (annealed at 400–500 °C for 0.5 h).

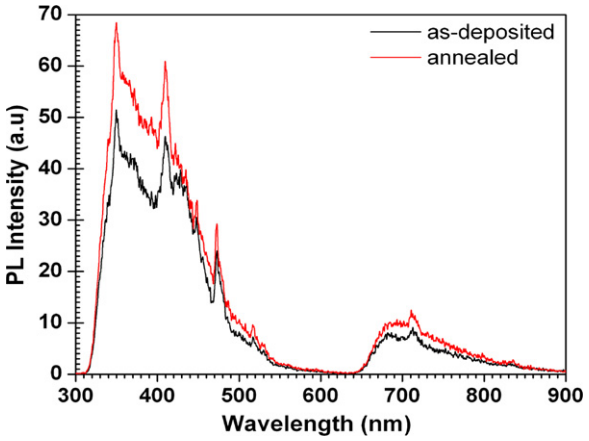

Fig. 12. PL spectra for the as-deposited sample and the annealed CuO NSs (annealed at 500 °C for 3 h).

Fig. 12 shows photoluminescence (PL) spectra for the as-deposited and annealed (at 500 °C for 3 h) samples. Emission peaks at 350 nm (3.55 eV), 410 nm (3.03 eV), 473 nm (2.62 eV) and 518 nm (2.40 eV) were observed in all samples, which indicated CuO emission [9,12,28–33]. It is noted that the peak centered at 430 nm (2.89 eV), which indicates Cu emission, did not appear in the annealed sample [11]. The PL peak located at 685 nm (1.81 eV) is related to the interstitial in CuO whereas the peak of 714 nm (1.74 eV) is related to the recombination of electrons and holes at oxygen vacancies [32–35]. However, the increase in PL intensity with increasing annealing temperature may be the result of a grain size growth and a crystallinity improvement, which is confirmed by TEM images (Fig. 7b and d) and the XRD result.

4. Conclusions

Cu/CuO NRs and their bundles were successfully synthesized on glass substrates by an electrochemical dissolution and deposition method. A steady current at an electrode separation of 8 mm and a voltage of 10 V for a deposition time of 1 h made uniform and smooth films. The morphology of CuO NRs and the ratio of bundles/NRs were observed by controlling the deposition time, the electrode separation and the voltage. An aggregation mechanism was used to explain the formation of the NRs and their bundles. The Cu phase of the as-deposited sample could be transformed to a sin-

gle CuO phase with monoclinic structure by annealing at 500 °C. PL spectra of the annealed samples showed an increase in magnitude as a result of grain size growth and an improvement in crystallinity. Thus, this research suggests a simple method for the preparation of many other metal/metal-oxide NSs.

Acknowledgements

We thank the National Research University Project under Thailand's Office of the Commission on Higher Education (CHE) for financial support and Graduate School Chiang Mai University. B. Toboonsung was supported by a grant from the CHE under the program of Strategic Scholarships for Frontier Research Network for the Join Ph.D. Program Thai Doctoral degree, Thailand.

References

[1] G. Papadimitropoulos, N. Vourdas, V.E.M. Vamvakas, D. Davazoglou, Thin Solid Films 515 (2006) 2428.
[2] Y. Liu, L. Liao, J. Li, C. Pan, J. Phys. Chem. C 111 (2007) 5050.
[3] S. Sumikaru, S. Mori, S. Shimizu, H. Usami, E. Suzuki, J. Photochem. Photobiol. A 194 (2008) 143.
[4] H. Zhang, M. Zhang, Mater. Chem. Phys. 108 (2008) 184.
[5] L. Liao, Z. Zhang, B. Yan, Z. Zheng, Q.L. Bao, T. Wu, C.M. Li, Z.X. Shen, J.X. Zhang, H. Gong, J.C. Li, T. Yu, Nanotechnology 20 (2009) 085203.
[6] J.C. Park, J. Kim, H. Kwan, H. Song, Adv. Mater. 21 (2009) 803.
[7] G. Ren, D. Hu, E.W.C. Cheng, M.A. Vargas-Reus, P. Reip, R.P. Allaker, Int. J. Antimicrob. Agents 33 (2009) 587.
[8] J. Xu, K. Yu, J. Wu, D. Shang, L. Li, Y. Xu, Z. Zhu, J. Phys. D: Appl. Phys. 42 (2009) 075417.
[9] I.Y. Erdogan, O. Gullu, J. Alloy Compd. 492 (2010) 378.
[10] S. Li, H. Zhang, Y. Ji, D. Yang, Nanotechnology 15 (2004) 1428.
[11] S.S. Chang, Mater. Chem. Phys. 86 (2004) 247.
[12] S.S. Chang, H.J. Lee, H.J. Park, Ceram. Int. 31 (2005) 411.
[13] K. Zhang, C. Rossi, C. Tenailleau, P. Alphonse, J.Y. Chane-Ching, Nanotechnology 18 (2007) 275607.
[14] R.P. Wijesundera, M. Hidaka, K. Koga, M. Sakai, W. Siripala, J.Y. Choi, N.E. Sung, Phys. Status Solidi B 244 (2007) 4629.
[15] G.N. Rao, Y.D. Yao, J.W. Chen, J. Appl. Phys. 105 (2009) 093901.
[16] A.H. Jayatissa, K. Guo, A.C. Jayasuriya, Appl. Surf. Sci. 255 (2009) 9474.
[17] A. Chen, G. Yang, H. Long, F. Li, Y. Li, P. Lu, Thin Solid Films 517 (2009) 4277.
[18] G.Q. Yuan, H.F. Jiang, C. Lin, S.J. Liao, J. Cryst. Growth 303 (2007) 400.
[19] X.Z. Lin, P. Liu, J.M. Yu, G.W. Yang, J. Phys. Chem. C 113 (2009) 17543.
[20] S. Sahoo, S. Husale, B. Colwill, T.-M. Lu, S. Nayak, P.M. Ajayan, ACS Nano 3 (2009) 3935.
[21] D.P. Singh, N.R. Neti, A.S.K. Sinha, O.N. Srivastava, J. Phys. Chem. C 111 (2007) 1638.
[22] Z. Zhang, H. Sun, X. Shao, D. Li, H. Yu, M. Han, Adv. Mater. 17 (2005) 42.
[23] R.L. Penn, J. Phys. Chem. B 108 (2004) 12707–12712.
[24] V. Figueriredo, E. Elangovan, G. Goncalves, P. Barquinha, L. Pereira, N. Franco, E. Alves, R. Martins, E. Fortunato, Appl. Surf. Sci. 254 (2008) 3949.
[25] T. Yu, C.H. Sow, A. Gantimahapatruni, F.C. Cheong, Y. Zhu, K.C. Chin, X. Xu, C.T. Lim, Z. Shen, J.T.L. Thong, A.T.S. Wee, Nanotechnology 16 (2005) 1238–1244.
[26] J. Zhu, H. Bi, Y. Wang, X. Wang, X. Yang, L. Lu, Mater. Chem. Phys. 109 (2008) 34–38.
[27] W. Wang, Y. Zhuang, L. Li, Mater. Lett. 62 (2008) 1724–1726.
[28] H.H. Lin, C.Y. Wang, H.C. Shih, J.M. Chen, C.T. Hsieh, J. Appl. Phys. 95 (2004) 5889.
[29] D.I. Son, C.H. You, T.W. Kim, Appl. Surf. Sci. 255 (2009) 8794.
[30] C.Y. Huang, A. Chatterjee, S.B. Liu, S.Y. Wu, C.L. Cheng, Appl. Surf. Sci. 256 (2010) 3688.
[31] C. Jin, K. Baek, S. Park, H.W. Kim, W.I. Lee, C. Lee, Solid State Commun. 150 (2010) 1812.
[32] A. Aslani, V. Oroojpour, Physica B 406 (2011) 144.
[33] A. Aslani, Physica B 406 (2011) 150.
[34] H. Solache-Carranco, G. Juarez-Diaz, A. Esparza-Garcia, M. Briseno-Garcia, M. Galvan-Arellano, J. Martinez-Juarez, G. Romero-Paredes, R. Pena-Sierra, J. Lumin. 129 (2009) 1483.
[35] P. Gao, M. Gu, X.L. Liu, B. Liu, S.M. Huang, Appl. Phys. Lett. 95 (2009) 221904.